Bragg solitons in systems with separated nonuniform Bragg grating and nonlinearity

Tanvir Ahmed and Javid Atai
School of Electrical and Information Engineering, The University of Sydney, NSW 2006, Australia
(Received 11 July 2017; published 20 September 2017)

The existence and stability of quiescent Bragg grating solitons are systematically investigated in a dual-core fiber, where one of the cores is uniform and has Kerr nonlinearity while the other one is linear and incorporates a Bragg grating with dispersive reflectivity. Three spectral gaps are identified in the system, in which both lower and upper band gaps overlap with one branch of the continuous spectrum; therefore, these are not genuine band gaps. However, the central band gap is a genuine band gap. Soliton solutions are found in the lower and upper gaps only. It is found that in certain parameter ranges, the solitons develop side lobes. To analyze the side lobes, we have derived exact analytical expressions for the tails of solitons that are in excellent agreement with the numerical solutions. We have analyzed the stability of solitons in the system by means of systematic numerical simulations. We have found vast stable regions in the upper and lower gaps. The effect and interplay of dispersive reflectivity, the group velocity difference, and the grating-induced coupling on the stability of solitons are investigated. A key finding is that a stronger grating-induced coupling coefficient counteracts the stabilization effect of dispersive reflectivity.

DOI: 10.1103/PhysRevE.96.032222

I. INTRODUCTION

Fiber Bragg gratings (FBGs) are produced as a result of the variation of the refractive index of the fiber core. In the past few decades, FBGs have received a great deal of attention due to their potential applications in sensing, dispersion compensation, switching, filtering, and pulse compression [1–8]. One of the main features of FBGs is that the cross-coupling between the forward- and backward-propagating waves opens a band gap in their spectrum within which linear waves cannot propagate. This also gives rise to a strong effective dispersion that can be up to six orders of magnitude greater than that of silica [9,10].

The existence of solitons in periodic structures was originally predicted in the context of superlattices [11]. In the case of FBGs, at sufficiently high intensities, Kerr nonlinearity can be counterbalanced by FBG-induced dispersion, resulting in the formation of Bragg grating (BG) solitons [10,12,13]. Theoretical studies have shown that in a uniform FBG, the BG solitons form a two-parameter family of solutions that fill the entire band gap [10,12,13]. One of the parameters is the soliton's velocity, which can range from zero to the speed of light in the medium. The other parameter is related to the detuning frequency, the width of the soliton, and the peak power. As for the stability of BG solitons, it has been demonstrated that approximately half of the soliton family is stable [14–16]. Extensive experimental effort has been devoted to observe slow BG solitons due to their potential applications [17–21]. Thus far, BG solitons with a velocity of 23% of the speed of light in the medium have been observed experimentally [22]. BG and gap solitons have been theoretically predicted and studied in other structures, such as photonic crystals [23–26], dual-core fibers [27–31], waveguide arrays [32–34], and microcavities with a periodic potential [35]. They have also been investigated in a variety of nonlinear media, including quadratic nonlinearity [36–38], sign-changing Kerr nonlinearity [39], and cubic-quintic nonlinearity [40–43].

Nonlinear couplers have received much attention during the past three decades due to their potential applications in signal processing and optical switching [44–49]. It has been shown that asymmetric nonlinear couplers (e.g., a coupler in which one core is linear and the other is nonlinear) exhibit interesting dynamics and characteristics [50–55]. It is therefore expected that grating-assisted nonlinear couplers may offer new possibilities for novel applications. For example, it has been shown that a semilinear dual-core fiber where one core is linear and the other has a Bragg grating and Kerr nonlinearity can support quiescent and moving solitons [27,56]. With regard to the fabrication of such gratings, they can be produced by writing the grating on one or both cores in the coupling region [57]. Such gratings can be used as add-drop elements in wavelength-division multiplexed (WDM) networks [58].

Nonstandard Bragg gratings such as Bragg superstructures [59,60], gratings written on photonic wires [61], and nonuniform gratings may possess broad and inhomogeneous band gaps. As a result, their analysis requires that the standard model be modified. In Ref. [62], it was shown that one way to deal with the effect of nonuniformity in FBGs is to modify the standard model so that the contribution of spatial dispersion of Bragg reflectivity is taken into account. A key finding was that the presence of dispersive reflectivity results in the expansion of the stability region for both quiescent and moving solitons [62,63].

In the vast majority of dual-core systems with gratings considered thus far, the Bragg grating and nonlinearity occur in the same core. In Ref. [28], a semilinear dual-core model was presented and analyzed. In that model, the linear core had a Bragg grating and the nonlinear core was uniform. In this case, the model's linear spectrum differs greatly from that of earlier models, and it was demonstrated that quiescent and moving solitons existed in such a system.

In this paper, we will generalize the model of Ref. [28] by incorporating dispersive reflectivity into the system, and we will systematically investigate the stability of quiescent solitons in the generalized model. The rest of the paper is as follows. In Sec. II, the model is introduced and its linear spectrum is analyzed. The characteristics of the soliton solutions and the analytical solutions for the solitons' side lobes are

presented in Sec. III. The stability of the solitons is discussed in Sec. IV. A summary of the results is presented in Sec. V.

II. THE MODEL

In Ref. [28], a model was presented for the propagation of light in a dual-core system comprised of a linear core equipped with *uniform* Bragg grating and a uniform nonlinear core with Kerr nonlinearity. The starting point for the derivation of the model of Ref. [28] is Maxwell's equations. One can then follow the steps for deriving the generalized massive Thirring model (GMTM) [10] and nonlinear coupled mode equations (see, e.g., Chap. 3 of Ref. [64]) to arrive at the model of Ref. [28]. One can also use a combination of multiple-scales analysis [65] and coupled-mode theory to derive the model. It should be noted that in the derivation of our model, the effects of birefringence (see, for example, [66]) are assumed to be negligible. Also, the effects of electrostrictive and acoustic waves [67] are ignored due to the fact that the length scales over which they occur are far greater than the length of a typical FBG. Following the procedure outlined in Ref. [62], the model of Ref. [28] can be generalized to include the effect of dispersive reflectivity in the linear core. This results in the following system of partial differential equations:

$$\begin{aligned} iu_t + iu_x + \left[|v|^2 + \tfrac{1}{2}|u|^2\right]u + \phi &= 0,\\ iv_t - iv_x + \left[|u|^2 + \tfrac{1}{2}|v|^2\right]v + \psi &= 0,\\ i\phi_t + ic\phi_x + u + \lambda\psi + m\psi_{xx} &= 0,\\ i\psi_t - ic\psi_x + v + \lambda\phi + m\phi_{xx} &= 0, \end{aligned} \tag{1}$$

where u and v denote the forward- and backward-propagating waves in the nonlinear core, and ϕ and ψ are their counterparts in the linear core, which contains a Bragg grating. The coefficient of linear coupling between the cores is normalized to be 1. λ is the Bragg-grating-induced linear coupling coefficient between the left- and right-propagating waves; λ is real and $\lambda > 0$. The group velocity in the nonlinear core is set equal to 1, and c represents the relative group velocity in the linear core. The parameter $m > 0$ is the dispersive reflectivity strength. Without loss of generality, the analysis is confined to $0 \leqslant m \leqslant 0.5$ since there is no practical importance for $m > 0.5$ [62].

As was mentioned earlier, dual-core systems with grating in one or both cores can be fabricated with the current technology. With regard to the realization of the model, the coupling length L_c and the Bragg reflection length L_B need to be of the same order of magnitude. Typically, L_B is of the order of 1 mm. Couplers with $L_c \sim 1$ mm can also readily be manufactured. In real units, $\Delta t = 1$ and $\Delta x = 1$ correspond to approximately 10 ps and 1 mm. Given that silica's nonlinear coefficient is $\sim 2\,(\text{km W})^{-1}$, the estimated peak power for soliton formation is estimated to be $\sim$1 MW. This is actually an upper bound. The experimental results show that the actual power needed to observe solitons is much less than this estimate [17–20]. Using these parameter values, the length of the dual-core system is estimated to be $\approx$10 cm.

The system's linear spectrum provides the essential information regarding the spectral gaps within which solitons may exist. Substituting $u, v, \phi, \psi \sim \exp(ikx - i\omega t)$ into the linearized form of Eqs. (1) results in the following dispersion relation:

$$\begin{aligned} &\omega^4 - [2 + (\lambda - mk^2)^2 + (1 + c^2)k^2]\omega^2\\ &\quad + (\lambda k - mk^3)^2 + (ck^2 - 1)^2 = 0. \end{aligned} \tag{2}$$

Equation (2) results in the following expression for the branches of the spectrum:

$$\omega^2 = 1 + \frac{m^2k^4 + (c^2 - 2\lambda m + 1)k^2 + \lambda^2}{2} \pm \frac{\sqrt{\{2 + (\lambda - mk^2)^2 + (1 + c^2)k^2\}^2 - 4\{(\lambda - mk^2)^2k^2 + (ck^2 - 1)^2\}}}{2}. \tag{3}$$

Further analysis of Eq. (3) shows that generally the spectrum consists of three disjoint band gaps: a central band gap surrounded by two other gaps—one in the upper half and the other in the lower half of the spectrum. The central gap is a genuine band gap. On the other hand, the upper and lower gaps overlap with one branch of the continuous spectrum, and therefore they are not genuine gaps. Examples of dispersion diagrams are shown in Fig. 1. In the special case of $m = 0$ and $c = 0$, Eq. (3) leads to the band gaps derived in Ref. [28], i.e., for $\lambda > \frac{1}{\sqrt{2}}$ the band gaps are given by

$$\lambda < \omega < \frac{\lambda}{2} + \frac{\sqrt{\lambda^2 + 4}}{2}, \tag{4}$$

$$\frac{\lambda}{2} - \frac{\sqrt{\lambda^2 + 4}}{2} < \omega < -\frac{\lambda}{2} + \frac{\sqrt{\lambda^2 + 4}}{2}, \tag{5}$$

$$-\frac{\lambda}{2} - \frac{\sqrt{\lambda^2 + 4}}{2} < \omega < -\lambda, \tag{6}$$

and for $\lambda < \frac{1}{\sqrt{2}}$ the band gaps are

$$-\frac{\lambda}{2} + \frac{\sqrt{\lambda^2 + 4}}{2} < \omega < \frac{\lambda}{2} + \frac{\sqrt{\lambda^2 + 4}}{2}, \tag{7}$$

$$-\lambda < \omega < \lambda, \tag{8}$$

$$-\frac{\lambda}{2} - \frac{\sqrt{\lambda^2 + 4}}{2} < \omega < \frac{\lambda}{2} - \frac{\sqrt{\lambda^2 + 4}}{2}. \tag{9}$$

When $\lambda = \frac{1}{\sqrt{2}}$, the three gaps merge into a single gap, i.e., $-\sqrt{2} < \omega < \sqrt{2}$.

The presence of dispersive reflectivity significantly alters the characteristics of the band gaps. First, the widths of the upper and lower band gaps remain independent of m (for $0 < m \leqslant 0.5$) and occur at $k = 0$ if $\lambda \lessapprox 0.55$. In this case, the upper

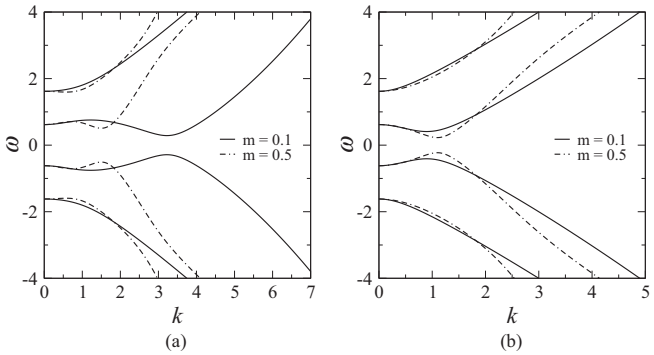

FIG. 1. Dispersion diagrams for different parameter values. (a) $c = 0.0, \lambda = 1.0$; (b) $c = 1.0, \lambda = 1.0$.

and lower band gaps are given by

$$-\frac{\lambda}{2}+\frac{\sqrt{\lambda^2+4}}{2}\leqslant\omega\leqslant\frac{\lambda}{2}+\frac{\sqrt{\lambda^2+4}}{2},$$
$$-\frac{\lambda}{2}-\frac{\sqrt{\lambda^2+4}}{2}\leqslant\omega\leqslant\frac{\lambda}{2}-\frac{\sqrt{\lambda^2+4}}{2}. \quad (10)$$

It is noteworthy that the width of the band gaps is equal to λ. For $\lambda \geqslant 0.55$, these band gaps decrease with increasing m at $c = 0$. However, increasing c prevents the narrowing of the band gaps. Also, as λ increases, larger values of c are required to maintain the band gap at a fixed value.

As for the central gap, its boundaries do not occur at $k = 0$ and its width must be determined numerically. The width of the central gap varies (i.e., increases or decreases even to zero) with increasing values of m for fixed values of c and λ. It should also be noted that the central band gap closes for all $c \neq 0$ when $m = c\lambda$.

As is shown in Fig. 1, Eq. (3) gives rise to four branches that are symmetric with respect to $\omega = 0$. In the absence of dispersive reflectivity (i.e., $m = 0$) at $|k| \to \infty$ the upper (lower) branch in the upper half plane of the dispersion diagram asymptotically approaches $\omega^2 \approx \max\{c^2, 1\}k^2$ ($\omega^2 \approx \min\{c^2, 1\}k^2$) for any values of $c \geqslant 0$ ($c > 0$). In the special case of $c = 0$, the lower branch asymptotically approaches $\omega^2 \approx \lambda^2$. In the presence of dispersive reflectivity (i.e., $m \neq 0$), the asymptotic form of these branches is independent of c. At $|k| = \infty$, the upper and lower dispersion branches in the case of $m \neq 0$ approach $\omega^2 \approx m^2k^4$ and $\omega^2 \approx k^2$, respectively, for any values of $c \neq 0$.

III. SOLITON SOLUTIONS

In the absence of dispersive reflectivity (i.e., $m = 0$), it has been shown that the model of Eqs. (1) admits exact analytical soliton solutions for $c = 0$. However, when $c \neq 0$ and/or $m \neq 0$ the solutions must be obtained numerically. We assume that the stationary solutions of the system are of the form $\{u(x,t), v(x,t)\} = \{U(x), V(x)\}\exp(-i\omega t)$ and $\{\phi(x,t), \psi(x,t)\} = \{\Phi(x), \Psi(x)\}\exp(-i\omega t)$. Substituting these expressions into Eqs. (1) and applying the symmetry condition $\{V(x), \Psi(x)\} = \{-U^*(x), -\Phi^*(x)\}$, we arrive at

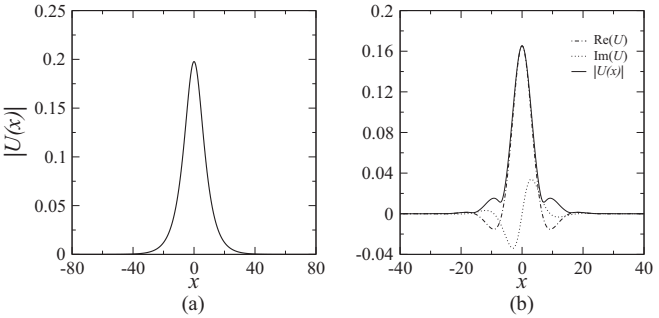

FIG. 2. Examples of soliton solutions at $\lambda = 1.0$, $c = 0.3$, and $\omega = 1.61$: (a) soliton without side lobes for $m = 0.1$ and (b) soliton with side lobes for $m = 0.5$.

the following system of ordinary differential equations:

$$\omega U + iU_x + \tfrac{3}{2}|U|^2U + \Phi = 0,$$
$$\omega\Phi + ic\Phi_x + U - \lambda\Phi^* - m\Phi^*_{xx} = 0. \quad (11)$$

To determine the quiescent soliton solutions, Eqs. (11) are solved by means of the relaxation algorithm. Stationary soliton solutions are found throughout the upper and lower gaps. However, no stationary soliton solutions exist in the central gap. It is also found that, up to available numerical accuracy, the soliton solutions in the upper and lower gaps form a continuous family of solutions. Similar to other systems with dispersive reflectivity (e.g., Refs. [62] and [68]), in certain parameter ranges, side lobes appear in the solitons' profiles. Typical examples of soliton solutions with and without side lobes are shown in Fig. 2.

Generally, the amplitudes of the side lobes are much smaller than that of the soliton. As a result, the effect of nonlinearity on the formation of side lobes is negligible. Therefore, to characterize the tails of the solitons, we linearize Eq. (11) to arrive at the following set of equations:

$$\omega U + i\frac{dU}{dx} + \Phi = 0,$$
$$\omega\Phi + ic\frac{d\Phi}{dx} + U - \lambda\Phi^* - m\frac{d^2\Phi^*}{dx^2} = 0. \quad (12)$$

Equations (11) can further be simplified by noting that $\Phi = -\omega U - idU/dx$ [see the first equation in Eqs. (12)], resulting in the following equation:

$$im\frac{d^3U^*}{dx^3} - m\omega\frac{d^2U^*}{dx^2} - c\frac{d^2U}{dx^2} + i\lambda\frac{dU^*}{dx}$$
$$+ i\omega(1+c)\frac{dU}{dx} - \lambda\omega U^* + (\omega^2-1)U = 0. \quad (13)$$

Substituting $U(x) = U_r(x) + iU_i(x)$ into Eq. (13) leads to the following system of ordinary differential equations:

$$m\frac{d^3U_r}{dx^3} - (c - m\omega)\frac{d^2U_i}{dx^2} + [\omega(1+c) + \lambda]\frac{dU_r}{dx}$$
$$+ [\lambda\omega + (\omega^2-1)]U_i = 0,$$
$$m\frac{d^3U_i}{dx^3} - (c + m\omega)\frac{d^2U_r}{dx^2} - [\omega(1+c) - \lambda]\frac{dU_i}{dx}$$
$$- [\lambda\omega - (\omega^2-1)]U_r = 0. \quad (14)$$

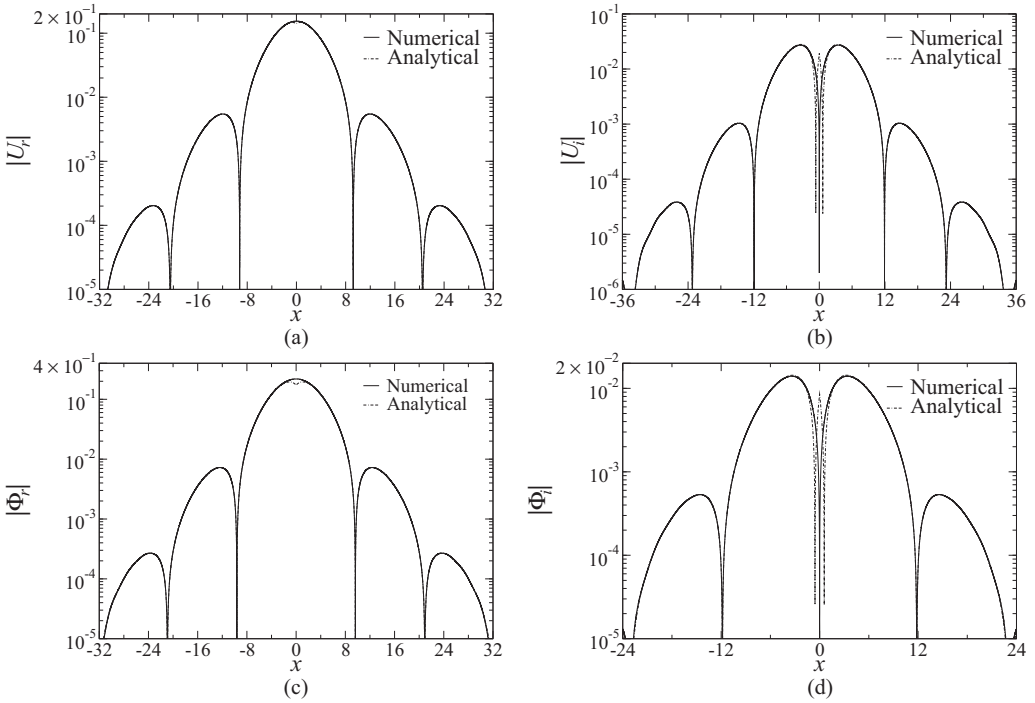

FIG. 3. Comparison between numerically obtained soliton solutions and analytical expressions for the tails of solitons [i.e., Eqs. (19) and the corresponding Φ_r and Φ_i are obtained from $\Phi = -\omega U - idU/dx$] for $\lambda = 0.8$, $\omega = 1.47$, $c = 0.1$, $m = 0.5$, $\alpha = 0.291$, and $\beta = 0.278$. The parameters in Eqs. (19) are determined from the numerical soliton solution and are found to be $A_1 = 0.260$, $A_2 = 0.108$, $\theta_1 = -0.997$, and $\theta_2 = -1.748$. The parameters α and β are calculated using Eqs. (16).

The characteristic equation of Eqs. (14) has the following form:

$$as^6 + bs^4 + ps^2 + q = 0, \tag{15}$$

where a, b, p, and q are real-valued quantities and are given by $a = m^2$, $b = m(m\omega^2 + 2\lambda) - c^2$, $p = \lambda^2 - (1 - 2\lambda m + c^2)\omega^2 - 2c$, and $q = \lambda^2\omega^2 - (\omega^2 - 1)^2$. The roots of Eq. (15) are given by

$$\begin{aligned} s_{1,2} &= \pm\sqrt{A - \frac{b}{3a} - \frac{B}{A}}, \\ s_{3,4} &= \pm\sqrt{\frac{B}{2A} - \frac{b}{3a} - \frac{A}{2} - \frac{\sqrt{3}}{2}\left(\frac{B}{A} + A\right)i}, \\ s_{5,6} &= \pm\sqrt{\frac{B}{2A} - \frac{b}{3a} - \frac{A}{2} + \frac{\sqrt{3}}{2}\left(\frac{B}{A} + A\right)i}, \end{aligned} \tag{16}$$

where $A = \sqrt[3]{\sqrt{C^2 + B^3} - C}$, $B = \frac{-b^2}{9a^2} + \frac{p}{3a}$, and $C = \frac{q}{2a} + \frac{b^3}{27a^3} - \frac{bp}{6a^2}$.

Equations (14) admit the following general solutions:

$$\begin{aligned} U_r(x) &= C_1 e^{-s_1 x} + C_2 e^{s_1 x} + C_3 e^{-s_3 x} + C_4 e^{s_3 x} \\ &\quad + C_5 e^{-s_5 x} + C_6 e^{s_5 x}, \\ U_i(x) &= D_1 e^{-s_1 x} + D_2 e^{s_1 x} + D_3 e^{-s_3 x} + D_4 e^{s_3 x} \\ &\quad + D_5 e^{-s_5 x} + D_6 e^{s_5 x}, \end{aligned} \tag{17}$$

where C_n and D_n $(n = 1,2,\ldots,6)$ are general arbitrary complex coefficients that need to be determined by the appropriate boundary conditions. The complex constants $\{C_1, C_3, C_5\}$ ($\{C_2, C_4, C_6\}$) and $\{D_1, D_3, D_5\}$ ($\{D_2, D_4, D_6\}$) correspond to the right (left) tail of $U_r(x)$ and $U_i(x)$, i.e., $x > 0$ ($x < 0$). Therefore, for the right tail (i.e., $x > 0$), the constants C_2, C_4, C_6, D_2, D_4, and D_6 must be zero. Similarly, the constants C_1, C_3, C_5, D_1, D_3, and D_5 must be zero for $x < 0$. Due to the symmetry of the soliton, $C_1 = C_2$, $C_3 = C_4$, $D_1 = D_2$, and $D_3 = D_4$. Additionally, since $U_r(x)$ and $U_i(x)$ are real-valued, $C_3 = C_1^*$ and $D_3 = D_1^*$. Our analysis shows that, in the range $0 < m \leqslant 0.5$, s_5 and s_6 are purely imaginary, and C_5, C_6, D_5, and D_6 are negligibly small. Therefore, Eqs. (17) can be simplified as follows:

$$\begin{aligned} U_r(x) &= C_1 e^{-s_1 x} + C_1 e^{s_1 x} + C_1^* e^{-s_3 x} + C_1^* e^{s_3 x}, \\ U_i(x) &= D_1 e^{-s_1 x} + D_1 e^{s_1 x} + D_1^* e^{-s_3 x} + D_1^* e^{s_3 x}. \end{aligned} \tag{18}$$

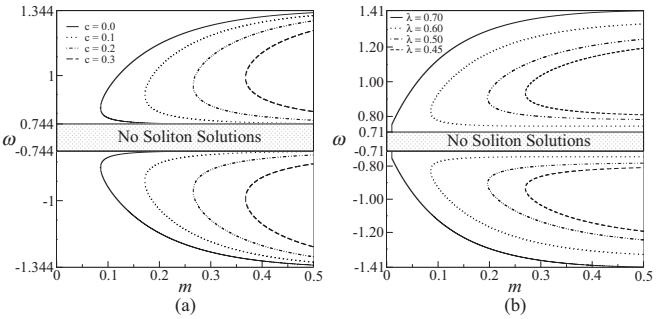

FIG. 4. The regions on the (m,ω) plane where solitons develop side lobes for (a) $\lambda = 0.6$ and (b) $c = 0$. The side lobes appear in the regions to the right of each curve.

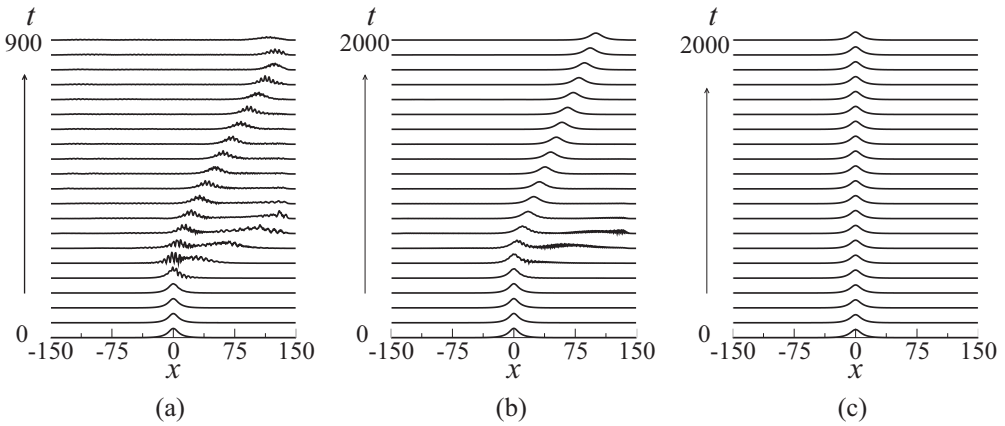

FIG. 5. Examples of the propagation of solitons for $\lambda = 0.2$, $c = 0.5$ with (a) an unstable soliton resulting in the soliton decay with $\omega = 0.98$ and $m = 0.3$; (b) an unstable soliton evolving to a moving soliton with $\omega = 0.98$ and $m = 0.1$; and (c) a stable soliton with $\omega = 1.01$ and $m = 0.1$. Only the $|u|$ component is shown.

When the exponents in Eqs. (18) are real, the tails of the soliton decay exponentially. On the other hand, side lobes are formed when the exponents in Eqs. (18) are complex. Substituting $s_1 = \alpha - j\beta$ and $s_3 = \alpha + j\beta$ in Eqs. (18) results in the following expressions for $U_r(x)$ and $U_i(x)$:

$$U_r(x) = A_1\{e^{-\alpha x}\cos(\beta x + \theta_1) + e^{\alpha x}\cos(-\beta x + \theta_1)\},$$
$$U_i(x) = A_2\{e^{-\alpha x}\cos(\beta x + \theta_2) - e^{\alpha x}\cos(-\beta x + \theta_2)\}. \tag{19}$$

The free real parameters A_1, A_2, θ_1, and θ_2 in Eqs. (19) are determined from the numerical soliton solutions and are related to C_1 and D_1 through $A_1 = 2|C_1|$, $A_2 = 2|D_1|$, $\theta_1 = \arg(C_1)$, and $\theta_2 = \arg(D_1)$. It should be noted that the first term in Eqs. (19) represents the right tail (i.e., $x > 0$), and the second term corresponds to the left tail (i.e., $x < 0$). The equations for Φ_r and Φ_i can readily be obtained by substituting $U(x) = U_r(x) + iU_i(x)$ into $\Phi = -\omega U - idU/dx$ [see the first equation in Eqs. (12)]. As is shown in Fig. 3, the numerically obtained soliton solutions and the analytical expressions for U_r, U_i, Φ_r, and Φ_i are in excellent agreement except in the vicinity of the soliton's peak, where the linear approximation does not hold.

We have also investigated the effects of c and λ on the formation of side lobes. Figure 4 depicts the typical regions where side lobes occur for different values of c and λ. A noteworthy feature shown in Fig. 4 is that, for a fixed $\lambda(c)$, the region where side lobes occur shrinks as $c(\lambda)$ increases (decreases).

IV. STABILITY ANALYSIS

To analyze the stability of solitons, we have performed a systematic numerical stability analysis by solving Eqs. (1) using the symmetrized split-step scheme for various values of m, c, and λ. In all simulations, the numerically obtained soliton solutions were propagated up to $t = 2000$. The inherent numerical noise was found to be sufficient to seed the onset of instability. Examples of stable and unstable solitons are shown in Fig. 5.

With regard to the dynamics of unstable solitons, unstable solitons that are deep in the unstable region strongly radiate and are deformed during propagation and subsequently decay into radiation [see, for example, Fig. 5(a)]. On the other hand, unstable solitons close to the stable region radiate some energy and subsequently rearrange themselves into another stable

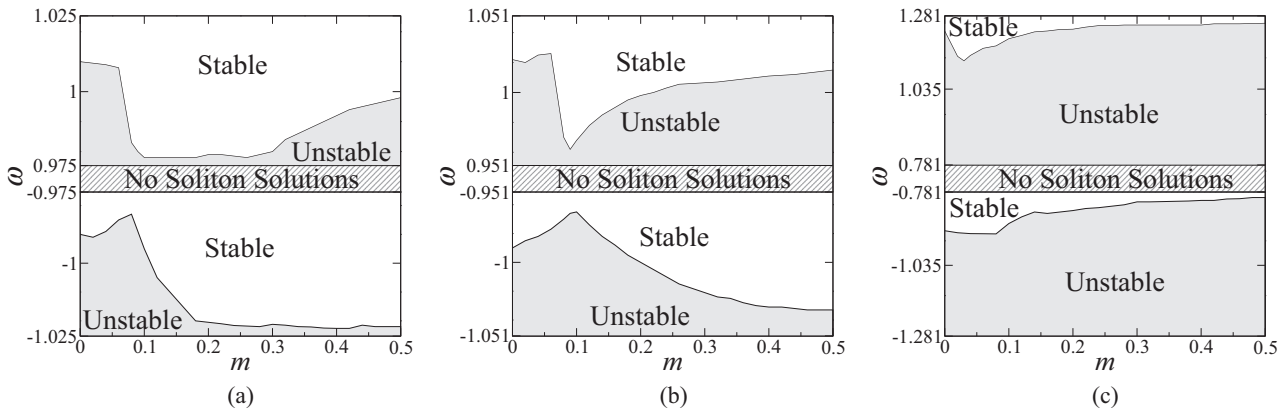

FIG. 6. Stability regions for $c = 0$ on the (m,ω) plane. (a) $\lambda = 0.05$, (b) $\lambda = 0.1$, and (c) $\lambda = 0.5$.

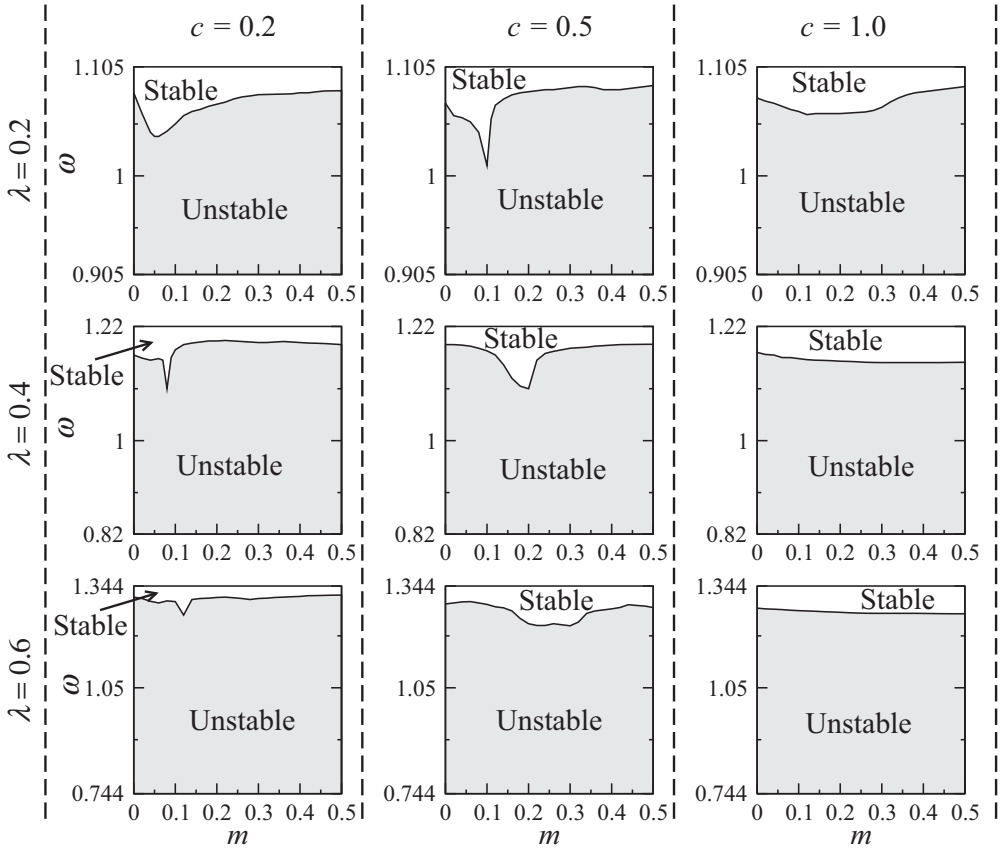

FIG. 7. Stability diagrams in the upper gap for different values of c and λ on the (m,ω) plane.

quiescent soliton or evolve into a stable moving soliton [see, for example, Fig. 5(b)]. These simulation results confirm that stable moving solitons exist in the model.

The results of simulations for various values of λ and $c = 0$ are presented in Fig. 6. A noteworthy trend shown in Fig. 6 is that as λ increases, the ratio of the size of the stable region relative to the size of the band gap (i.e., area of the stable region/area of the band gap) in both the upper and lower gaps decreases. In other words, the stabilization of solitons due to dispersive reflectivity is mitigated by increasing λ.

In the case of $c \neq 0$, we have systematically investigated the stability of solitons for various values of c and λ. The results of the stability analysis for the upper and lower band gaps are summarized, respectively, in Figs. 7 and 8. A general trend shown in Figs. 7 and 8 is that, for a fixed c, as λ increases the ratio of the size of the stable region to the size of the band gap is reduced. This is consistent with the results of Fig. 6.

As for the effect of c, in the upper gap for moderate values of λ (i.e., $\lambda = 0.4$ and 0.6), as c is increased from 0.2 to 1 the stable region enlarges. However, for $\lambda = 0.2$, increasing c from 0.2 to 0.5 leads to the enlargement of the stable region, but a further increase to $c = 1$ results in the shrinkage of the stable region. In the lower gap, the opposite behavior is observed, i.e., for $\lambda = 0.2$, increasing c gives rise to the expansion of the stable region. But for $\lambda = 0.4$ and 0.6, increasing c from 0.2 to 0.5 enlarges the stable region, and with a further increase of c the stable region shrinks.

In some of the stability diagrams in the upper gap, a cusp is formed (e.g., the diagram corresponding to $\lambda = 0.2$ and $c = 0.5$ in Fig. 7). Our analysis shows that the cusp corresponds to $m = c\lambda$.

V. CONCLUSION

We have investigated the existence and stability of quiescent solitons in a dual-core system where one core is uniform and has Kerr nonlinearity and the other is linear and equipped with a Bragg grating with dispersive reflectivity. The linear spectrum of the model has three band gaps for all values of c, namely an upper band gap, a lower band gap, and a central one. Since the upper and lower band gaps overlap with a branch of the continuous spectrum, they are not genuine band gaps. The central band gap, however, is a genuine band gap.

Soliton solutions are not found in the central band gap, but they exist as a continuous family throughout the upper and lower band gaps. It is found that, depending on the value of c and λ, above a certain value of m solitons develop side lobes in their profiles. We have derived exact analytical expressions for the tails of the solitons. The analytical expressions and numerical solutions are found to be in excellent agreement. We have analyzed the effect of c and λ on the side-lobe formation. It has been shown that for a given $\lambda(c)$, the region in the (m,ω) plane where side lobes occur shrinks as $c(\lambda)$ increases (decreases).

We have investigated the stability of the solitons systematically for different values of m, c, and λ. We have identified

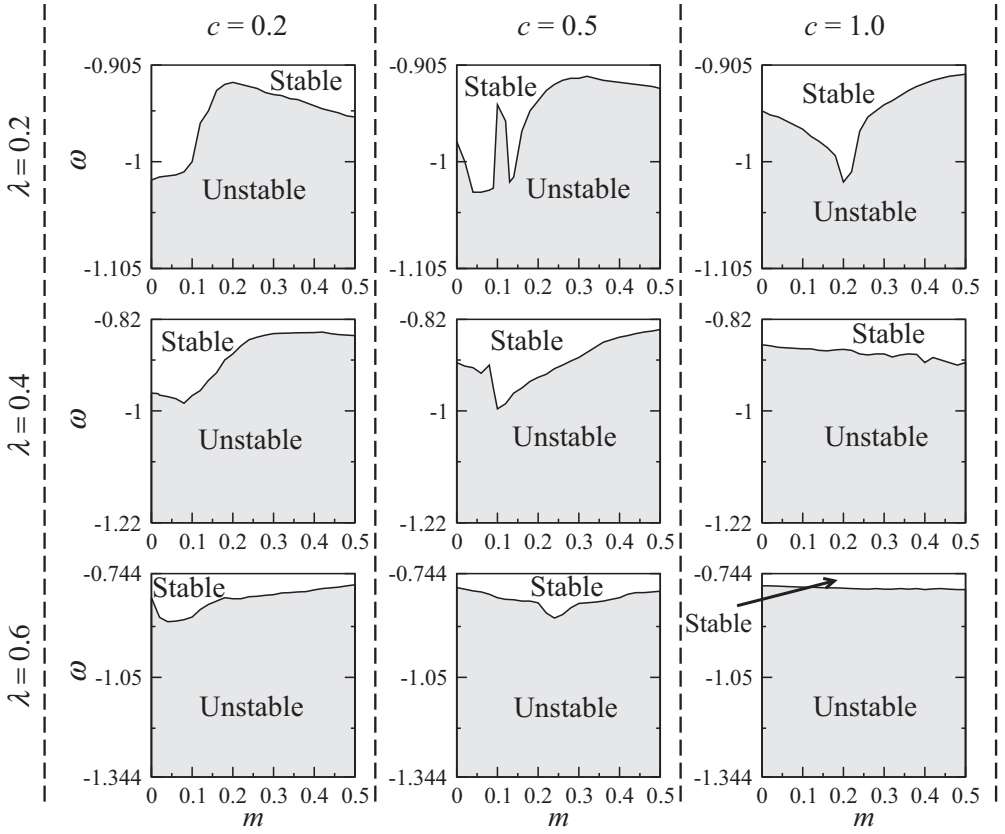

FIG. 8. Stability diagrams in the lower gap for different values of c and λ on the (m,ω) plane.

nontrivial stability borders in the plane of (m,ω), and we investigated the effect of the system parameters on the stability of solitons. A general finding is that, in both upper and lower gaps, higher values of λ for both $c = 0$ and $c \neq 0$ lead to a reduction in the size of the stable region relative to the size of the gap.

[1] R. Kashyap, *Fiber Bragg Gratings* (Academic Press, San Diego, 1999).
[2] P. A. Krug, T. Stephens, G. Yoffe, F. Ouellette, P. Hill, and G. Dhosi, Electron. Lett. **31**, 1091 (1995).
[3] S. Radic, N. George, and G. P. Agrawal, J. Opt. Soc. Am. B **12**, 671 (1995).
[4] W. H. Loh, R. I. Laming, N. Robinson, A. Cavaciuti, F. Vaninetti, C. J. Anderson, M. N. Zervas, and M. J. Cole, IEEE Photon. Technol. Lett. **8**, 944 (1996).
[5] H. G. Winful, J. H. Marburger, and E. Garmire, Appl. Phys. Lett. **75**, 379 (1979).
[6] N. D. Sankey, D. F. Prelewitz, and T. G. Brown, Appl. Phys. Lett. **60**, 1427 (1992).
[7] S. LaRochelle, Y. Hibino, V. Mizrahi, and G. I. Stegeman, Electron. Lett. **26**, 1459 (1990).
[8] H. Cao, J. Atai, X. Shu, and G. Chen, Opt. Express **20**, 12095 (2012).
[9] P. S. J. Russell, J. Mod. Opt. **38**, 1599 (1991).
[10] C. M. de Sterke and J. E. Sipe, Progr. Opt. **33**, 203 (1994).
[11] W. Chen and D. L. Mills, Phys. Rev. Lett. **58**, 160 (1987).
[12] D. N. Christodoulides and R. I. Joseph, Phys. Rev. Lett. **62**, 1746 (1989).
[13] A. B. Aceves and S. Wabnitz, Phys. Lett. A **141**, 37 (1989).
[14] B. A. Malomed and R. S. Tasgal, Phys. Rev. E **49**, 5787 (1994).
[15] I. V. Barashenkov, D. E. Pelinovsky, and E. V. Zemlyanaya, Phys. Rev. Lett. **80**, 5117 (1998).
[16] A. De Rossi, C. Conti, and S. Trillo, Phys. Rev. Lett. **81**, 85 (1998).
[17] B. J. Eggleton, C. M. de Sterke, and R. E. Slusher, J. Opt. Soc. Am. B **14**, 2980 (1997).
[18] B. J. Eggleton, R. E. Slusher, C. M. de Sterke, P. A. Krug, and J. E. Sipe, Phys. Rev. Lett. **76**, 1627 (1996).
[19] C. M. de Sterke, B. J. Eggleton, and P. A. Krug, J. Lightwave Technol. **15**, 1494 (1997).
[20] D. Taverner, N. G. R. Broderick, D. J. Richardson, R. I. Laming, and M. Ibsen, Opt. Lett. **23**, 328 (1998).
[21] B. J. Eggleton, C. M. de Sterke, and R. E. Slusher, J. Opt. Soc. Am. B **16**, 587 (1999).
[22] I. C. M. Littler, J. T. Mok, B. J. Eggleton, and C. M. de Sterke, Nat. Phys. **2**, 775 (2006).
[23] C. Monat, C. M. de Sterke, and B. J. Eggleton, J. Opt. **12**, 104003 (2010).
[24] D. V. Skryabin, Opt. Express **12**, 4841 (2004).

[25] J. Atai, B. A. Malomed, and I. M. Merhasin, Opt. Commun. **265**, 342 (2006).
[26] D. R. Neill and J. Atai, Phys. Lett. A **367**, 73 (2007).
[27] J. Atai and B. A. Malomed, Phys. Rev. E **62**, 8713 (2000).
[28] J. Atai and B. A. Malomed, Phys. Rev. E **64**, 066617 (2001).
[29] W. C. K. Mak, P. L. Chu, and B. A. Malomed, J. Opt. Soc. Am. B **15**, 1685 (1998).
[30] W. C. K. Mak, B. A. Malomed, and P. L. Chu, Phys. Rev. E **69**, 066610 (2004).
[31] Y. J. Tsofe and B. A. Malomed, Phys. Rev. E **75**, 056603 (2007).
[32] D. Mandelik, R. Morandotti, J. S. Aitchison, and Y. Silberberg, Phys. Rev. Lett. **92**, 093904 (2004).
[33] Y. Tan, F. Chen, P. P. Beličev, M. Stepić, A. Maluckov, C. E. Rüter, and D. Kip, Appl. Phys. B **95**, 531 (2009).
[34] R. Dong, C. E. Rüter, D. Kip, J. Cuevas, P. G. Kevrekidis, D. Song, and J. Xu, Phys. Rev. A **83**, 063816 (2011).
[35] A. V. Gorbach, B. A. Malomed, and D. V. Skryabin, Phys. Lett. A **373**, 3024 (2009).
[36] C. Conti, S. Trillo, and G. Assanto, Phys. Rev. Lett. **78**, 2341 (1997).
[37] H. He and P. D. Drummond, Phys. Rev. Lett. **78**, 4311 (1997).
[38] W. C. K. Mak, B. A. Malomed, and P. L. Chu, Phys. Rev. E **58**, 6708 (1998).
[39] J. Atai and B. A. Malomed, Phys. Lett. A **298**, 140 (2002).
[40] J. Atai and B. A. Malomed, Phys. Lett. A **284**, 247 (2001).
[41] J. Atai, J. Opt. B **6**, S177 (2004).
[42] S. Dasanayaka and J. Atai, Phys. Lett. A **375**, 225 (2010).
[43] S. Dasanayaka and J. Atai, Phys. Rev. E **84**, 026613 (2011).
[44] S. M. Jensen, IEEE Trans. Microwave Theory Technol. **30**, 1568 (1982).
[45] A. A. Maier, Sov. J. Quantum Electron. **12**, 1490 (1982).
[46] A. A. Maier, Sov. J. Quantum Electron. **14**, 101 (1984).
[47] B. Daino, G. Gregori, and S. Wabnitz, J. Appl. Phys. **58**, 4512 (1985).
[48] H. E. Nistazakis, D. J. Frantzeskakis, J. Atai, B. A. Malomed, N. Efremidis, and K. Hizanidis, Phys. Rev. E **65**, 036605 (2002).
[49] Y. Chen and J. Atai, Opt. Commun. **150**, 381 (1998).
[50] S. Trillo and S. Wabnitz, Appl. Phys. Lett. **49**, 752 (1986).
[51] J. Atai and Y. Chen, J. Appl. Phys. **72**, 24 (1992).
[52] J. Atai and Y. Chen, IEEE J. Quantum Electron. **29**, 242 (1993).
[53] M. Bertolotti, M. Monaco, and C. Sibilia, Opt. Commun. **116**, 405 (1995).
[54] D. J. Kaup, T. I. Lakoba, and B. A. Malomed, J. Opt. Soc. Am. B **14**, 1199 (1997).
[55] W. B. Fraga, J. W. M. Menezes, M. G. da Silva, C. S. Sobrinho, and A. S. B. Sombra, Opt. Commun. **262**, 32 (2006).
[56] R. Shnaiderman, R. S. Tasgal, and Y. B. Band, Opt. Lett. **36**, 2438 (2011).
[57] J.-L. Archambault, P. S. J. Russell, S. Barcelos, P. Hua, and L. Reekie, Opt. Lett. **19**, 180 (1994).
[58] M. Åslund, L. Poladian, J. Canning, and C. M. de Sterke, J. Lightwave Technol. **20**, 1585 (2002).
[59] B. J. Eggleton, P. A. Krug, L. Poladian, and F. Ouellette, Electron. Lett. **30**, 1620 (1994).
[60] N. G. R. Broderick and C. M. de Sterke, Phys. Rev. E **55**, 3634 (1997).
[61] M. Gnan, G. Bellanca, H. M. H. Chong, P. Bassi, and R. M. De La Rue, Opt. Quantum Electron. **38**, 133 (2006).
[62] J. Atai and B. A. Malomed, Phys. Lett. A **342**, 404 (2005).
[63] D. R. Neill, J. Atai, and B. A. Malomed, J. Opt. A **10**, 085105 (2008).
[64] D. Marcuse, *Theory of Dielectric Optical Waveguides* (Academic Press, San Diego, 1991).
[65] J. W. Haus, B. Y. Soon, M. Scalora, C. Sibilia, and I. M. Mel'nikov, J. Opt. Soc. Am. B **19**, 2282 (2002).
[66] A. Macho, C. García-Meca, F. Fraile-Peláez, M. Morant, and R. Llorente, Opt. Express **24**, 021415 (2016).
[67] E. Dianov, A. Luchnikov, A. Pilipetskii, and A. Starodumov, Opt. Lett. **15**, 314 (1990).
[68] S. A. M. S. Chowdhury and J. Atai, IEEE J. Quantum Electron. **50**, 458 (2014).